J. Math. Biol.
DOI 10.1007/s00285-012-0612-z

Mathematical Biology

Seasonal forcing and multi-year cycles in interacting populations: lessons from a predator–prey model

Rachel A. Taylor · Jonathan A. Sherratt · Andrew White

Received: 23 August 2012 / Revised: 8 October 2012

Abstract Many natural systems are subject to seasonal environmental change. As a consequence many species exhibit seasonal changes in their life history parameters—such as a peak in the birth rate in spring. It is important to understand how this seasonal forcing affects the population dynamics. The main way in which seasonal models have been studied is through a two dimensional bifurcation approach. We augment this bifurcation approach with extensive simulation in order to understand the potential solution behaviours for a predator–prey system with a seasonally forced prey growth rate. We consider separately how forcing influences the system when the unforced dynamics have either monotonic decay to the coexistence steady state, or oscillatory decay, or stable limit cycles. The range of behaviour the system can exhibit includes multi-year cycles of different periodicities, parameter ranges with coexisting multi-year cycles of the same or different period as well as quasi-periodicity and chaos. We show that the level of oscillation in the unforced system has a large effect on the range of behaviour when the system is seasonally forced. We discuss how the methods could be extended to understand the dynamics of a wide range of ecological and epidemiological systems that are subject to seasonal changes.

Keywords Predator–prey · Seasonal forcing · Multi-year cycles · Subharmonics · Bifurcation diagram · Cyclic populations

Mathematics Subject Classification (2000) 34A34 · 92B05

R. A. Taylor (✉) · J. A. Sherratt · A. White
Department of Mathematics and the Maxwell Institute for Mathematical Sciences,
Heriot-Watt University, Edinburgh EH14 4AS, UK
e-mail: rat3@hw.ac.uk

Published online: 09 November 2012

1 Introduction

Many natural systems are subject to significant seasonal fluctuations in their life history parameters. This has been studied in the context of epidemiology, and seasonal forcing has been proposed as the cause of multi-year cycles for a number of diseases in human and wildlife populations (Dietz 1976; Finkenstadt and Grenfell 2000; Dushoff et al. 2004; Altizer et al. 2006; Keeling and Rohani 2008; Smith et al. 2008). Literature on interacting populations which include seasonal forcing is also plentiful. Interacting population systems can often cycle without forcing, implying a richer range of potential effects of seasonality, and conclusions from previous studies indicate that seasonal forcing can have critical effects on the population behaviour (Scheffer et al. 1997; Holt and Colvin 1997; Stenseth et al. 1998; Mabille et al. 2010).

The main mathematical approach to investigating the effects of seasonal forcing in epidemiological and ecological models is the bifurcation approach of Rinaldi and co-workers (Kuznetsov et al. 1992; Rinaldi et al. 1993; Rinaldi and Muratori 1993; Kuznetsov and Piccardi 1994; Kuznetsov 1995) and continued by others (Mancusi et al. 2004; Bolzoni et al. 2008). This uses numerical bifurcation software to construct bifurcation diagrams of solution behaviour as the forcing parameters are varied. It provides a systematic method for investigating solution structure and revealing all possible solutions. However, when there are multiple stable solutions, it gives no information on the relative frequency with which these arise. Alternative approaches include the resonance approach pioneered by Greenman (Greenman et al. 2004; Ireland et al. 2004; Greenman and Norman 2007; Greenman and Pasour 2011) and bifurcation analysis in the manner of King and Schaffer (1999, 2001) and Schaffer et al. (2001). The resonance approach constructs resonance diagrams to demonstrate increases in solution amplitude when the forcing period and the underlying period of the unforced system are integer multiples of one another. The approach used by King and Schaffer examines the bifurcation structure by formulating the model as a perturbation of a Hamiltonian limit, and then presents the work through a combination of two-dimensional bifurcation diagrams and sections of the Poincaré map.

In this paper, we will focus on the bifurcation approach to understand solution behaviour and augment it by a systematic program of numerical simulations in order to give more information on basins of attraction. We consider the specific case of the Rosenzweig–MacArthur predator–prey model with sinusoidal forcing of the prey growth rate. In reality, biological systems are very complex with the likelihood that all parameters are in some way affected by the seasons but with different forcing strengths and phases. We assume that the growth rate varies while the carrying capacity remains constant. This reflects the situation where the host has a defined breeding season but resources remain constant (and therefore breeding and resources are driven by different environmental factors). This differs to the work of Rinaldi et al. (1993) who applied temporal forcing to the growth rate and additionally forced the carrying capacity (with the same temporal forcing term). The prey growth rate is distinguished as the only model parameter that does not affect the stability of the predator–prey coexistence equilibrium (details in Sect. 2) thus allowing us to study the effects of the forcing from a different perspective, namely studying the three cases of monotonic decay to the coexistence equilibrium, oscillatory decay and cycles in the unforced system

separately. This provides a novel outlook on the impact of seasonal forcing, illustrating how the resulting cyclic behaviour is dependent on the unforced dynamics.

In Sect. 2 we describe the predator–prey model, its properties in the unforced case, and the different forcing scenarios we will consider. In Sect. 3 we summarise the necessary bifurcation theory, and the results of this bifurcation approach follow in Sect. 4. Simulation work is shown in Sect. 5 while in Sect. 6 we consider the importance of our choices for a controlling parameter. In Sect. 7, we discuss how the methods support and verify each other as well as possible extensions and applications.

2 Model

We consider the widely used Rosenzweig–MacArthur predator–prey model (Rosenzweig and MacArthur 1963):

$$\frac{dx}{dt} = r\left(1 - \frac{x}{K}\right)x - \frac{axy}{b+x} \tag{1a}$$

$$\frac{dy}{dt} = \frac{caxy}{b+x} - dy \tag{1b}$$

where $x(t)$ and $y(t)$ are the prey and predator density at time t. All parameters are positive; r and K represent the growth rate and carrying capacity of the prey population respectively; d is the natural death rate for the predator population; and c relates birth of new predators to prey intake. The Holling Type II predation term is a saturating function in which a is the maximum predation rate and b is the density of prey at which the predation rate is half its maximum.

The model (1) has a coexistence steady state which is stable when:

$$K_1 \equiv \frac{bd}{ca-d} < K < \frac{b(ca+d)}{ca-d} \equiv K_2. \tag{2}$$

There is a transcritical bifurcation at $K = K_1$ denoting a change to the prey-only equilibrium; at $K = K_2$ there is a supercritical Hopf bifurcation, and a stable limit cycle arises. For $K_1 < K < K_2$ there is either monotonic decay or oscillatory decay to equilibrium, with oscillatory decay occurring for larger K, say $K > K^* \in (K_1, K_2)$ (see Fig. 1). Notice that the growth rate r is significant as the only parameter not involved in the formula for K_1 and K_2; however, r does affect K^* and the values of x and y at the steady state.

We introduce yearly forcing through the growth rate of the prey and following many previous studies (Rinaldi et al. 1993; Dietz 1976; Greenman et al. 2004; Choisy et al. 2006; He and Earn 2007) we use a sinusoidal form:

$$r(t) = r_0(1 + \epsilon \sin(2\pi t)). \tag{3}$$

When $\epsilon = 0$ then the seasonally forced model collapses to the unforced case with $r_0 = r$. Throughout, we will use r to denote the growth rate in the unforced system, with $r(t)$ being the growth rate in the forced system and r_0 being the mean value

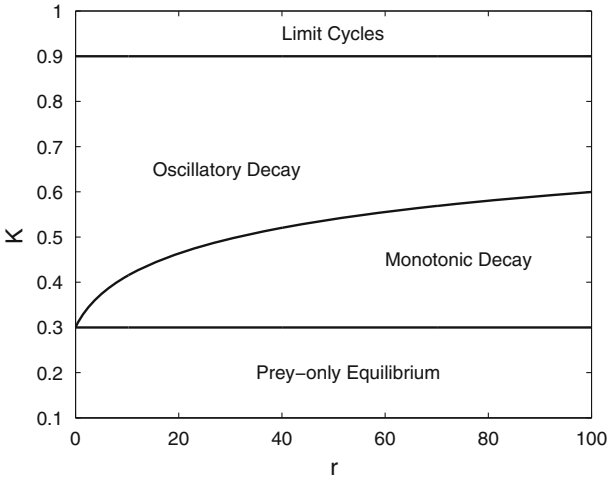

Fig. 1 The change in stability of the coexistence steady state as r and K vary. The other parameters are fixed at $a = 4\pi, b = 0.3, c = 1, d = 2\pi$. The switch between monotonic decay and oscillatory decay ($K = K^*$) increases with r. As $r \to \infty$, $K^* \to K_2 = 0.9$

of the growth rate in the forced system. This is to emphasise when we are referring to the unforced case. The parameter ϵ is the forcing amplitude. We will vary the two parameters in the forcing term, r_0 and ϵ, for fixed values of the other parameter values; following Rinaldi et al. (1993) we choose $a = 4\pi$, $b = 0.3$, $c = 1$, $d = 2\pi$. For these values $K_1 = 0.3$ and $K_2 = 0.9$.

We will focus on three different values of K : $K = 1$, giving a stable limit cycle in the unforced system; $K = 0.8$, giving oscillatory decay to the coexistence equilibrium; and $K = 0.35$, giving monotonic decay unless r_0 is small. We can consider these three cases separately because the threshold value K_2 is independent of the forcing parameter. Therefore we can analyse how the strength of oscillations in the unforced system affects the complexity of behaviour when seasonality is introduced.

3 Bifurcation theory of periodically forced ODEs

For the benefit of readers unfamiliar with the bifurcation theory of periodically forced ODEs, we now give a brief summary. Kuznetsov (1995) provides full details of all bifurcation theory necessary while Seydel (1994) and Guckenheimer and Holmes (1983) are perhaps more accessible for those unfamiliar with the theory. Useful background on Arnol'd Tongues is given in Greenman and Benton (2004) and King and Schaffer (1999). The standard procedure for locating bifurcations uses the Poincaré (or stroboscopic) map $\mathcal{P}$ that transforms the continuous system into a discrete one by sampling the solution once in each forcing period; one year in our case. Note that the stable/unstable annual cycles become stable/unstable fixed points of $\mathcal{P}$. Discrete bifurcation theory reveals that this fixed point is unstable if one of the eigenvalues of its linearisation has modulus larger than 1. Changes in stability are of three possible

types. If the eigenvalue is equal to -1, it is a *period-doubling (flip) bifurcation*; if the eigenvalue is equal to $+1$ it is a *fold (saddle-node, tangent) bifurcation*; and if there is a pair of complex conjugate eigenvalues with modulus 1, it is a *Neimark–Sacker (torus) bifurcation*.

Period-Doubling Bifurcation At a period-doubling bifurcation, the fixed point of $\mathcal{P}$ loses stability but no new fixed points appear. However, the same fixed point of the second iterate of $\mathcal{P}$ ($\mathcal{P}^2$) undergoes a pitchfork bifurcation leading to two fixed points of $\mathcal{P}^2$. Thus the solution alternates between two different points on the Poincaré section. For the continuous system this produces a two year cycle, which will typically become more distinctively biennial as one moves away from the bifurcation. A period-doubling bifurcation can then happen to the new two year cycles leading to a four year cycle, etc; this can yield an infinite cascade of period-doublings, ultimately ending in chaos. On our bifurcation diagrams, we will denote by PDk a period-doubling bifurcation curve across which a stable cycle of period k loses stability and a stable cycle of period $2k$ arises.

Fold Bifurcation When the eigenvalue is +1 the system undergoes a fold bifurcation. On one side of the bifurcation point there is no solution but on the other side there are both stable and unstable solution branches, which curve around ("fold") at the bifurcation point. By stability, we mean locally stable as a solution to the ODEs. Thus, when crossing a fold curve on the bifurcation diagram, a new solution appears to arise from nowhere. In fact, it is arising when the forcing period ($p = 1$ year) and the underlying period of the model (denoted by p_0) have the ratio $\frac{p}{p_0} = \frac{1}{n}$ ($n \in \mathbb{N}$). These bifurcations are the boundaries of Arnol'd Tongues, with each tongue denoting a region in which a specific periodic solution occurs. Thus, when crossing a fold bifurcation curve on the bifurcation diagram, denoted by FDk, a stable cycle of period k arises.

Neimark–Sacker Bifurcation A Neimark–Sacker bifurcation is a discrete version of a Hopf bifurcation. For a standard supercritical Neimark–Sacker bifurcation, when the eigenvalues are complex with modulus 1 the fixed point on the Poincaré section becomes unstable and a stable closed invariant curve arises around the point on the Poincaré section (provided that certain non-degeneracy conditions hold including that strong resonances should be excluded). If this is a space-filling curve, that is, if there is no number l such that l iterations of the Poincaré map $\mathcal{P}$ will bring the solution back to the same point on the curve, then it produces a *quasi-periodic* solution. More precisely, this means that the points of the solution on the Poincaré section are dense within this closed invariant curve. When considered in the continuous setting, a quasi-periodic solution may superficially appear periodic but in fact it has no finite period. The Neimark–Sacker bifurcation is also known as a torus bifurcation, due to the shape produced as it goes around the Poincaré section. Far away from the bifurcation point, the torus can undergo torus destruction leading to an area of chaotic behaviour, caused by a global bifurcation.

The condition for the closed invariant curve in the Poincaré map to be a space-filling curve is that the ratio of the two frequencies describing motion along the axis and along the cross-section of the torus is irrational. This ratio is the same as that between the

forcing period and the underlying period of the unforced model, which we discussed earlier. Due to the larger cardinality of irrational numbers over rational numbers, quasi-periodicity is the typical behaviour beyond a Neimark–Sacker bifurcation curve in the bifurcation diagram. This bifurcation curve is denoted by NSk where it is a cycle of period k which loses stability.

If the two frequencies have a rational ratio $\frac{m}{n}$ then there is *phase-locking* or *frequency-locking*. The solution becomes entrained on a periodic cycle within the curve on the Poincaré section and the period of the solution will be given by n. For example, if the forcing period and the underlying period have a ratio of $\frac{1}{3}$, then the system will respond with a solution of period 3. The fold bifurcation discussed earlier also gives phase-locking, with $m = 1$. As in the $m = 1$ case, solutions with a given $m \neq 1$ (and $n > 1$) occur within an Arnol'd Tongue, whose boundaries are fold bifurcations of the solution within the tongue. The fact that m can now take any positive integer value leads to different "families" of tongues which are numerated by m. However, the family with $m = 1$ usually has the largest tongue on the bifurcation diagram. Thus, period ratios of $\frac{2}{3}$ and $\frac{1}{3}$ will both produce 3 year solutions within their respective Arnol'd Tongue, but the latter will usually be more prominent in the bifurcation diagram (see later, Fig. 3b, where several FDk curves representing different Arnol'd Tongues are plotted). Typically, most tongues are so thin that they are difficult to find via simulation.

Finally in this section, we comment that throughout the paper we will use the term "subharmonics" to refer to any solution which has a period that is an integer multiple of the external forcing period (Seydel 1994). As the external period in question is one year, subharmonics will be multi-year cycles of period 2, 3, 4 years etc. Therefore, both the period-doubling and fold bifurcations produce subharmonics. We state this explicitly because confusion can arise from the fact that period-doubling bifurcations are sometimes called subharmonic bifurcations. Further, subharmonics are often described as being associated with the ratio of the different periods interacting, although this is only really true for the fold bifurcation and not the period-doubling bifurcation.

4 The bifurcation approach

We used the software package AUTO (Doedel 1981; Doedel et al. 1991, 2006; Doedel and Oldeman 2009) to calculate bifurcation diagrams for (1). We describe separately the results for $K = 0.8$ (oscillatory decay), $K = 1$ (limit cycles) and $K = 0.35$ (monotonic decay). We restrict attention almost entirely to $\epsilon < 1$, which guarantees that the prey growth rate is always positive.

4.1 Two-dimensional bifurcation diagram for $K = 0.8$

Figure 2 shows a bifurcation diagram in the ϵ–r_0 plane; recall that ϵ is the forcing amplitude and r_0 is the mean of the forced growth rate.

For low levels of forcing (i.e. small ϵ), there are yearly solutions in region 0, which emulate the forcing oscillation. As ϵ is increased a period-doubling curve is

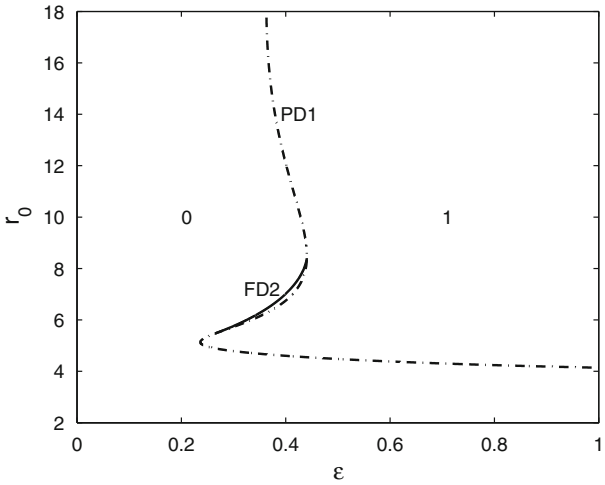

Fig. 2 A two-dimensional bifurcation diagram for $K = 0.8$ when the unforced system has oscillatory decay to the coexistence steady state. The two parameters varied in the diagram are those involved in the forcing term (Eq. 3), that is the mean value of the forcing, r_0, and the amplitude of the forcing, ϵ. The other parameters are $a = 4\pi$, $b = 0.3$, $c = 1$, $d = 2\pi$, $K = 0.8$. *Dot-dash lines* represent period-doubling bifurcation curves while *solid lines* are for fold bifurcation curves. In region 0 the system responds to the forcing with yearly cycles but after crossing the period-doubling curve PD1, indicating that a cycle of period 1 loses stability, the solution behaviour is two year cycles (region 1). The fold bifurcation curve shows an area where two year cycles can occur outside of the period-doubling region, thus between the two curves both the one year and the two year solutions are stable

crossed and thus the stable solution in region 1 is a two year cycle; the yearly solution also exists but is unstable. There is a fold bifurcation curve which implies a (small) region of parameter space outside the period-doubling region 1, containing two year solutions. The yearly solutions are also stable in this region: they do not lose stability until the period-doubling bifurcation curve is crossed. Thus between the two curves there are two different stable solutions. This is the full range of behaviour possible for when $K = 0.8$ as there are no more fold bifurcation curves for higher period cycles. However, in Sect. 5, we produce detailed simulation diagrams to investigate the basins of attraction for Fig. 2.

4.2 Two-dimensional bifurcation diagram for $K = 1$

The two-dimensional bifurcation diagram for the case $K = 1$ (stable limit cycles) is shown in Fig. 3 with and without the Arnol'd Tongues related to solutions of period greater than 2. Note that when r_0 is varied with no forcing ($\epsilon = 0$), the period of the limit cycles increases with decreasing r_0.

Figure 3a shows that a larger range of complex population behaviour is possible compared to when there is oscillatory decay in the unforced system (Fig. 2). A Neimark–Sacker bifurcation curve, labelled as NS1 occurs for this set-up. As we increase ϵ from 0 in a system with a limit cycle, the system typically responds with quasi-periodic solutions due to the appearance of the Neimark–Sacker bifurcation,

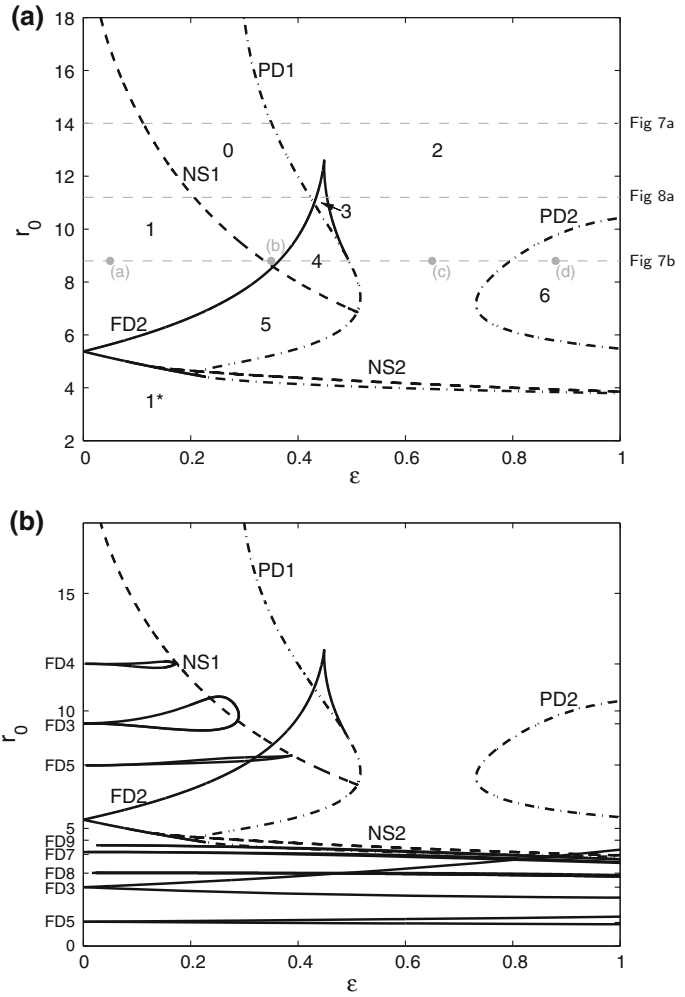

Fig. 3 A two-dimensional bifurcation diagram for $K = 1$ when the unforced system has stable limit cycles. Other parameters and details of the bifurcation diagram are as in Fig. 2. *Dot-dash lines* represent period-doubling bifurcation curves, *solid lines* are for fold bifurcation curves and *dashed lines* represent Neimark–Sacker bifurcation curves. **a** Stable behaviour by region: region 0—one year solution; region 1/1*—quasi-periodic cycles; region 2—two year solution; region 3—two different two year solutions; region 4—one year and two year solutions; region 5—quasi-periodic solution and two year solution; region 6—four year solution. *Grey dashed lines* refer to one-dimensional bifurcation diagrams in the relevant figures. Points (a)–(d) refer to the simulations shown in Fig. 4. **b** This includes the fold bifurcation curves relating to all multi-year simulations found. There are two FD3 curves indicating the appearance of three year cycles in different regions, one FD4 curve, two FD5, one FD7, FD8 and FD9 curves. We believe that the fold curves FD8 and FD9 do in reality extend to the $\epsilon = 0$ axis, with the earlier end a numerical artefact

and this is the generic behaviour in regions 1 and 1*. These quasi-periodic solutions will be very similar, for very low levels of forcing, to the limit cycles on the $\epsilon = 0$ axis, but increasing forcing pushes the solutions away from this period. Crossing the NS1 curve from region 1 to region 0 leads to the torus disappearing and the yearly

cycle becoming stable. Therefore the stable behaviour in region 0 is one year cycles. This implies that increasing the level of forcing is actually able to produce more regular behaviour—stable yearly cycles rather than quasi-periodicity. Although counter-intuitive, this does make sense as we are imposing yearly forcing on to an inherent cyclic solution (limit cycle) and with enough forcing, i.e. once ϵ is large enough, this cycle becomes entrained onto the yearly cycle. Note that if r had been part of condition (2) for a Hopf bifurcation, then the Neimark–Sacker bifurcation curve would have hit the $\epsilon = 0$ axis at the value of r where the Hopf bifurcation occurs.

As for $K = 0.8$, crossing from region 0 to region 2 across the period-doubling bifurcation curve PD1 leads to stable two year cycles in region 2 and the loss of stability of the yearly cycles. This new two year cycle itself undergoes period-doubling as indicated by the curve PD2. Thus the stable solution behaviour in region 6 is four year cycles. There is another period-doubling curve PD4, and a subsequent cascade of period-doubling to chaos, in the region $\epsilon > 1$. There is also a second Neimark–Sacker bifurcation curve, NS2, in region 2. As r_0 decreases past this curve, it indicates the loss of stability of the two year cycles in region 2 and the onset of stable quasi-periodic solutions. However, this region is very thin and further decrease in r_0 causes a loss of stability due to crossing the period-doubling curve PD1.

Thus in Fig. 3a there are four main types of behaviour shown on this two-dimensional bifurcation diagram, namely one year, two year, four year and quasi-periodic cycles. There is also the possibility that there may be chaotic dynamics in some parts of the "quasi-periodic regions"; we have not investigated this. Examples of these behaviours are shown in Fig. 4; the corresponding parameters sets are labelled (a)–(d) in Fig. 3a.

We now consider Fig. 3b which includes the higher period Arnol'd Tongues. We used simulation in order to obtain initial conditions as starting solutions for numerical continuation. Specifically we input into AUTO one whole period of the solution from a Matlab simulation and trace the solution branch to see what bifurcations occur along it, in particular the fold bifurcation curve enclosing the periodic solutions.

We see that the three year fold curve which has a root on the $\epsilon = 0$ axis at approximately $r_0 = 3$ is the largest of these additional tongues. However, there are many different period solutions, as well as multiple regions of the same period solution. In Fig. 5 we explore the two separate regions of three year stability by showing a representative solution from each of these regions, plotted as a function of time. Recall that a tongue is characterised by the rotation number $\frac{m}{n}$ within the torus. Here n is the period and m is the number of peaks in the solution per period. Thus the three year simulations found in Fig. 5a have $m = 1, n = 3$ while Fig. 5b corresponds to $m = 2, n = 3$. However, this rotation number also relates to the forcing period (1 year) and the underlying period of the unforced system. The larger 3 year fold curve hits the axis where the unforced system has a period of 3 years, thus leading to this rotation number of $\frac{1}{3}$. Furthermore, the smaller three year fold curve hits the axis at $r_0 = 9.5$ when the unforced system has a period of 1.5 years. Thus the rotation number is $\frac{1}{1.5} = \frac{2}{3}$ as expected.

This rotation number relationship is the same for all the Arnol'd tongues in Fig. 3b and we show this in Fig. 6. For example, the four year tongue on Fig. 3b touches the $\epsilon = 0$ axis where the limit cycles have period 1.25 so that the solution has

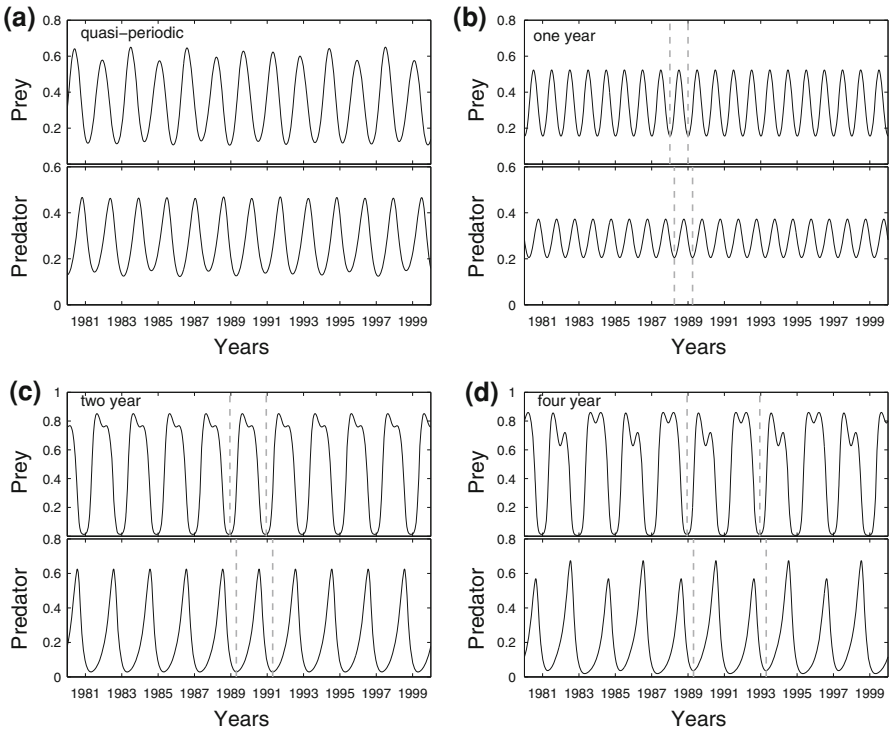

Fig. 4 Simulation examples of different solutions found through the bifurcation diagram approach. Parameter values are $(\epsilon, r_0) = (\mathbf{a})\ (0.05, 8.8)$, $(\mathbf{b})\ (0.35, 8.8)$, $(\mathbf{c})\ (0.65, 8.8)$, $(\mathbf{d})\ (0.88, 8.8)$ and correspond to the four points labelled on Fig. 3a with other parameters as in Fig. 3 ($K = 1$). The prey and predator solutions are plotted against time (years), with the simulations run for 2000 years so that they have settled to equilibrium. The Matlab ode solver (ode15s) was run with tolerances: reltol $= 10^{-8}$ and abstol $= 10^{-6}$. *Grey dashed lines* highlight a full period of the solution. The initial conditions were $(x_0, y_0) = (0.3, 0.3)$ in all cases

$\frac{m}{n} = \frac{1}{1.25} = \frac{3}{4}$. Thus we state $\frac{m}{n} = \frac{\text{peak}}{\text{period}}$ for each of the plots in Fig. 6(a)–(f) respectively, as $\frac{3}{4}, \frac{1}{5}, \frac{3}{5}, \frac{3}{7}, \frac{3}{8}, \frac{4}{9}$. These cycles may of course change in qualitative behaviour (although still being of the same period) as the ϵ and r_0 values move closer to the edge of the Arnol'd Tongue. In particular, the quasi-periodic behaviour near the tongue often looks similar to the periodic solution at the edge of the tongue.

Figure 3b shows a large number of tongues close to the $\epsilon = 0$ axis, and in fact general theory implies that there are an infinite number (see Sect. 3 and Kuznetsov 1995). However, in practice for small ϵ most of the tongues are very thin and the corresponding cycles will actually be very similar to the nearby quasi-periodic cycles. As ϵ increases, the tongues usually get thicker and the cycles begin to be more distinctively multi-year. Note also that in principle period-doubling can occur within the tongues. However, we have only found this within the three year fold near $r_0 = 3$, leading to six year cycles, and this occurs for $\epsilon > 1$. Also there are more Neimark–Sacker bifurcation curves which we did not calculate to avoid even more complexity on the diagram.

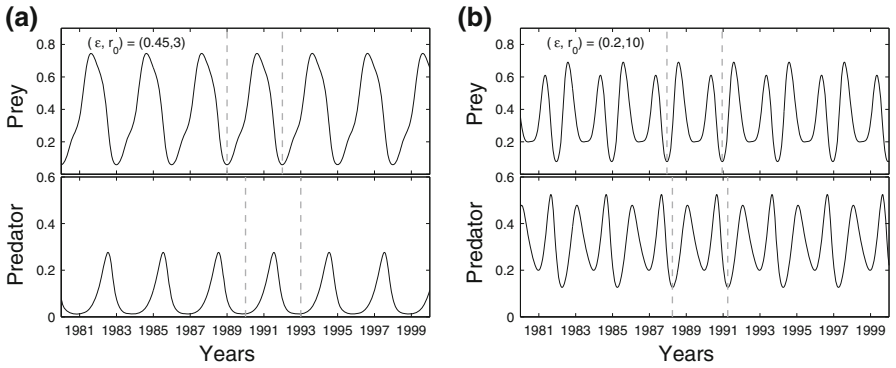

Fig. 5 Two different simulations of three year solutions. The simulations are taken from two different regions on the bifurcation diagram in Fig. 3b. The prey and predator solutions are plotted against time (years), with the simulations run for 2000 years so that it will have settled to equilibrium. The ode solver (ode15s) was run with tolerances: reltol $= 10^{-8}$ and abstol $= 10^{-6}$. Initial conditions were taken as $(x_0, y_0) = (0.5479, 0.7230)$ and $(0.1440, 0.6490)$. *Grey dashed lines* highlight a full period of the solution. The number of peaks over each three year period indicates which Arnol'd tongue the solutions belong to

General theory also implies that close to the $\epsilon = 0$ axis the Arnol'd tongues are non-overlapping since they are each governed by a different ratio of underlying period to forcing period at the root of the tongue (Kuznetsov 1995). However, for larger ϵ overlap can occur because the ratio determines only the root and period of the tongue; this is seen easily in Fig. 3b where the seven, eight and nine year tongues overlap the three year tongue. The points where different bifurcation curves intersect, for example where the fold curve FD2 hits the period-doubling curve PD1, are called codimension-two bifurcation points. These are flagged when tracing the curves in AUTO, indicating the presence of other bifurcation curves and providing a useful tool for finding all curves on the bifurcation diagram. The theory behind codimension-two bifurcation curves is well developed (see Kuznetsov 1995).

4.3 One-dimensional bifurcation diagrams for $K = 1$

We wish to analyse more closely the area enclosed by the fold bifurcation curve FD2 in Fig. 3a, where there are stable two year cycles. To do this, we switch to one-dimensional bifurcation diagrams, plotting the size (L_2-Norm) of the prey population against ϵ, for fixed r_0. We compare the solution behaviour when crossing the period-doubling curve PD1 for different values of r_0, in order to clarify how the fold bifurcation interacts with the period-doubling bifurcation.

When $r_0 = 14$ the fold curve is not present, and results show a supercritical period-doubling bifurcation, with the additional region of instability of the yearly cycle due to the Neimark–Sacker bifurcation (for $\epsilon < 0.12$) (Fig. 7a). Once the yearly solution becomes stable, $\epsilon > 0.12$, it remains stable until it hits the period-doubling bifurcation curve ($\epsilon = 0.35$). At this point the yearly solution becomes unstable and a stable two year cycle arises.

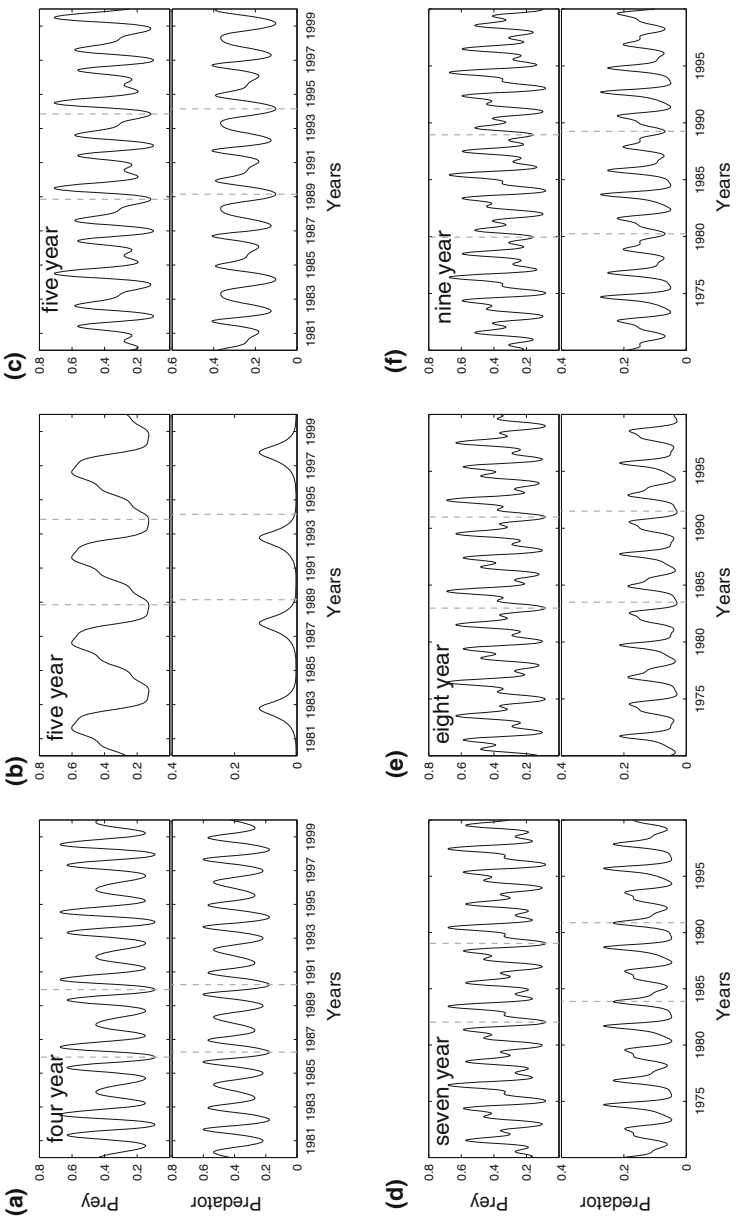

Fig. 6 Examples of solutions found in the bifurcation diagram for the case $K = 1$ (Fig. 3b). Parameter values are $(\epsilon, r_0) =$ (**a**) (0.1, 12), (**b**) (0.5, 1), (**c**) (0.3, 8), (**d**) (0.7, 3.8), (**e**) (0.95, 3), (**f**) (0.65, 4) and the cycle period for each case is indicated in each subplot. The prey and predator solutions are plotted against time (years). Further details are in Fig. 5. *Grey dashed lines* highlight a full period of the solution. Two different five year solutions are shown as two different regions of five year solution behaviour were found. Note that the time scale differs between cases as does the predator density plotting range. Initial conditions were taken as $(x_0, y_0) = (0.3, 0.3)$ except for the seven year cycles (0.8147, 0.9058) and eight year cycles (0.3448, 0.2718)

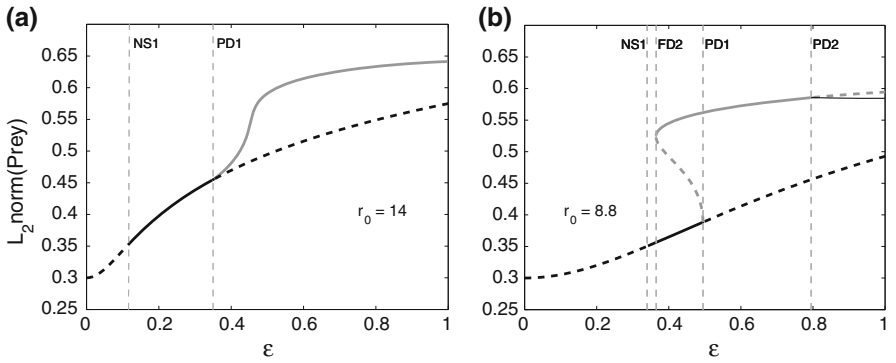

Fig. 7 A one-dimensional bifurcation diagram for fixed r_0 and varying ϵ with the other parameters as in Fig. 3a ($K = 1$). Along the vertical axis is the L_2-Norm of the prey solution. *Thick black curves*: 1 year equilibria, *thick grey curves*: 2 year equilibria, *thin black curves*: 4 year equilibria. *Solid curves* are stable while *dotted curves* are unstable. In (**a**) a supercritical period-doubling bifurcation occurs while in (**b**) the period-doubling bifurcation is subcritical and the solution then undergoes a fold. The *thin grey dashed lines* indicate when curves on the two-dimensional bifurcation diagram are crossed, labelled appropriately

When $r_0 = 8.8$ (Fig. 7b), we see a similar profile for the yearly cycle, going from unstable to stable to unstable as it first crosses the Neimark–Sacker bifurcation curve and then the period-doubling bifurcation curve. However, there is a marked change in the behaviour of the two year cycle. Again it bifurcates from the yearly cycle at the period-doubling bifurcation curve ($\epsilon = 0.49$), but now the bifurcation is subcritical. Thus it is initially unstable and only exists for $\epsilon < 0.49$, until it folds (at $\epsilon = 0.36$), at which point it becomes stable. Thus for values of ϵ between the fold bifurcation curve and the period-doubling bifurcation curve ($0.36 < \epsilon < 0.49$) there are two stable solutions—a one year solution and a two year solution. Lastly, Fig. 7b shows that for larger ϵ the two year cycle loses stability (at $\epsilon = 0.8$) and a stable four year cycle appears. This arises from crossing the period-doubling curve PD2.

Further understanding of the fold curve in Fig. 3a can be gained by examining a one-dimensional bifurcation diagram for $r_0 = 11.2$ (Fig. 8a). In particular, variation in ϵ will mean that region 3 in Fig. 3a will be explored. For $\epsilon < 0.4$ the one year solution has a similar behaviour to that shown in Fig. 7 (unstable, stable and then unstable due to the Neimark–Sacker bifurcation and the period-doubling bifurcation). In Fig. 8a one can see that the two year solution arises and is stable from the period-doubling bifurcation at $\epsilon = 0.42$. It then undergoes two folds giving it an "S shape" before continuing for increasing ϵ as a stable solution. More precisely, it hits the fold bifurcation curve FD2 twice, at $\epsilon = 0.435$ and $\epsilon = 0.452$. In Fig. 3a, this is reflected by the fact that region 3 is bounded on both sides by the fold curve FD2. Thus for $0.42 < \epsilon < 0.435$ and $\epsilon > 0.452$ there is one stable two year solution, whereas for $0.435 < \epsilon < 0.452$ there are two stable two year solutions. Examples of the two different two year solutions are shown in Fig. 8b,c for the prey population; these solutions are for the same parameter values but different initial conditions.

From the above one-dimensional bifurcation diagrams, one can see that increasing ϵ leads to an increase in the L_2-Norm of the solution and in that sense the two year

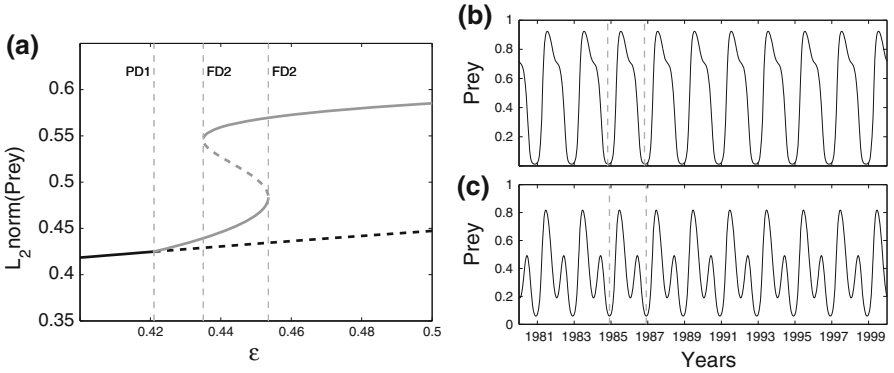

Fig. 8 Exploring region 3 in Fig. 3a. In (**a**) there is a one-dimensional bifurcation diagram for $r_0 = 11.2$, focussed in on $0.4 < \epsilon < 0.5$; behaviour outside this range is similar to Fig. 7a. A stable two year cycle appears when the yearly solution hits the PD1 curve. This undergoes two "folds", with instability in between, before continuing as a stable solution. Two stable two year solutions are shown in (**b**) and (**c**) with the same parameter values $(\epsilon, r_0) = (0.44, 11.2)$ but different initial conditions; namely (**b**)$(x_0, y_0) = (0.8245, 0.5211)$ and (**c**)$(x_0, y_0) = (0.9189, 0.7191)$. Here, the prey population is plotted against time over an interval of 20 years, once the solution has settled to equilibrium. For details on the numerical method see Fig. 4

cycle is larger than the one year cycle. This is also seen in Fig. 4 and complements the work of Greenman et al. (2004) and others (e.g. Bolzoni et al. 2008; Childs and Boots 2010). It ties in with the resonance peaks seen on Greenman's resonance diagram: subharmonics are a type of "resonant solution", with a higher amplitude than that of the applied forcing (Choisy et al. 2006). However, it should also be noted that the four year cycle is smaller in L_2-Norm than the two year cycle. This can be understood by looking at Fig. 4c, d where the two solutions have similar amplitude except that the four year solution only reaches this value every other peak.

4.4 Two-dimensional bifurcation diagram for $K = 0.35$

We now consider the final case of monotonic decay to the coexistence steady state. We have mentioned previously the importance of the interaction between the oscillations in the unforced model and the forcing term as a driver of complex behaviour. Thus, it is expected that the lack of any oscillations in the unforced model will cause the system to respond simply by emulating the forcing term. Both bifurcation and simulation analysis for $K = 0.35$ indicate that yearly cycles are the only possible population behaviour. A plot of the period-doubling curve (PD1) for different values of K (Fig. 9) indicates that the period-doubling region reduces in size as K decreases and entirely disappears at a value of K slightly greater than 0.6. As discussed in Sect. 2, the value K^* at which there is a switch from monotonic to oscillatory decay in the unforced model is an increasing function of r, with $K^* < 0.6$ throughout the range of values of $r(t) = r_0(1+\epsilon \sin(2\pi t))$ that we are considering. Thus, the period-doubling curve has disappeared while the system is still oscillatory and so one does not expect multi-year cycles in the monotonic decay regime.

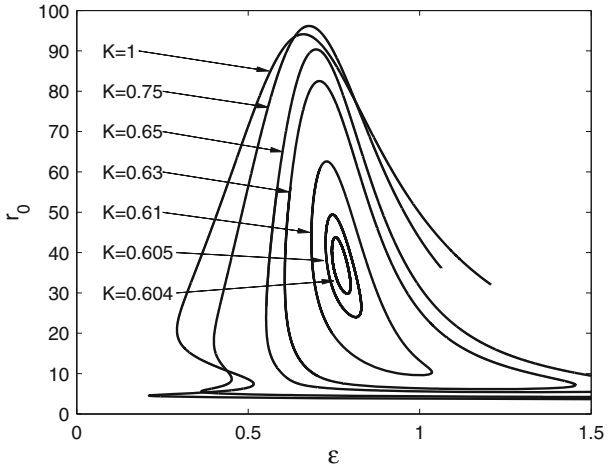

Fig. 9 Investigating whether complex behaviour can occur when the unforced system has monotonic decay to the coexistence steady state. The period-doubling curve indicating the appearance of stable two year solutions is drawn in the two-dimensional bifurcation diagram for decreasing values of K. As K decreases towards 0.6, the curve shrinks

This result suggests that a reasonable level of oscillatory decay is necessary in order for forcing to induce population behaviour that is more complex than annual cycles. If the period-doubling curve does not exist then the two year fold curve (FD2) also cannot exist. Further, we have not found Arnol'd tongues for these values of K (e.g. Fig. 12, below). This suggests that yearly cycles are the only possible behaviour when annual forcing is introduced into the system with monotonic decay to steady state.

4.5 AUTO details

The bifurcation diagrams discussed in this section were created in AUTO (Doedel 1981; Doedel et al. 1991, 2006; Doedel and Oldeman 2009) using essentially standard numerical continuation techniques. However, a few complications are worth mentioning. (i) We impose periodic forcing by augmenting (1) with a decoupled pair of ODEs which have an oscillatory solution of the form required for the forcing (Doedel and Oldeman 2009, §14.5). (ii) We found that versions of AUTO earlier than 07p-0.8 (2011) were not capable of continuing the Neimark–Sacker bifurcation curve. (iii) Although it can be useful to overspecify parameters so that it is always possible to see clearly the r_0 and ϵ values and to extract data easily, it has to be remembered that this is not possible when tracing the Neimark–Sacker bifurcation curve since AUTO will assume that a fourth specified parameter relates to the rotation angle around the torus. (iv) When trying to trace the period-doubling, fold and Neimark–Sacker bifurcation curves it is important to use a small step size so that the restart point for tracing the curve is determined accurately. Otherwise AUTO tends to have problems tracing the bifurcation curve from the restart point. (v) The labels for our curves were chosen to be Period-Doubling—PD, Fold—FD and Neimark–Sacker—NS. In AUTO the corresponding labels are PD, LP and TR respectively.

5 Simulation

This section will produce simulations of the model equations in order to elucidate the results presented in the bifurcation diagrams. In the previous section the bifurcation diagrams showed that there exist regions which have more than one type of possible solution behaviour. Simulation results can be used to estimate the likelihood of each of the solutions i.e. the relative sizes of their basins of attraction. Thus, simulation can expand our knowledge of subharmonic solutions. A comparison of the simulation results and bifurcation diagrams can therefore provide a clearer understanding of how forcing drives the population dynamics.

5.1 Simulation details

The predator–prey model equations (1) were solved using Matlab (ode15s) for 2,000 years and the solutions were tested to determine whether there was a periodic solution with period 1–9 years; if not, the solution was taken to be quasi-periodic. The choice of 9 years as a maximum test period is arbitrary; there could in principle be solutions with any finite integer period, but an upper limit is required for numerical study. To test whether a solution had a period of, for example, four years, the value of the prey solution was recorded for 20 time points at intervals of 4 years, after an initial time period of sufficient length that transients had decayed. If the difference between the maximum and minimum of these numbers was less than 2.5 % of their mean value, then it was declared a four year solution. Tests of some difficult cases near bifurcation curves or within multiple solution regions led to the choice of 2,000 years run time, 20 test points and 2.5 % variation as they enabled periodic and quasi-periodic solutions to be distinguished. We also investigated the use of the fast Fourier transform to find power spectra as a means of calculating the period but it was found to be less effective. We considered the parameter region $1 < r_0 < 20, 0 < \epsilon < 1$. For each set of parameter values, solutions were replicated 50 times using different (random) initial conditions between 0 and 1, independently chosen for both prey and predator. We determine the basins of attraction by examining the frequency of particular solutions from these 50 simulations. However, points in parameter space which showed multiple attractors were recomputed with 500 simulations to gain increased accuracy of the relative sizes of the basins of attractions. This straightforward method for estimating basins of attraction is effective (particularly as numerical investigations indicate that the basins of attraction have a complicated profile). Other, more sophisticated methods such as using Lyapunov functions (Giesl 2007) could also be used.

5.2 Simulation results for $K = 0.8$

Again we first explore the simpler case of when there is oscillatory decay to the coexistence steady state. In this case the two-dimensional bifurcation diagram (Fig. 2) showed only two types of behaviour—one year cycles and two year cycles.

Figure 10a shows the results from the $K = 0.8$ simulation program. Again, the only behaviours to occur are one year cycles (light blue) and two year cycles (pink).

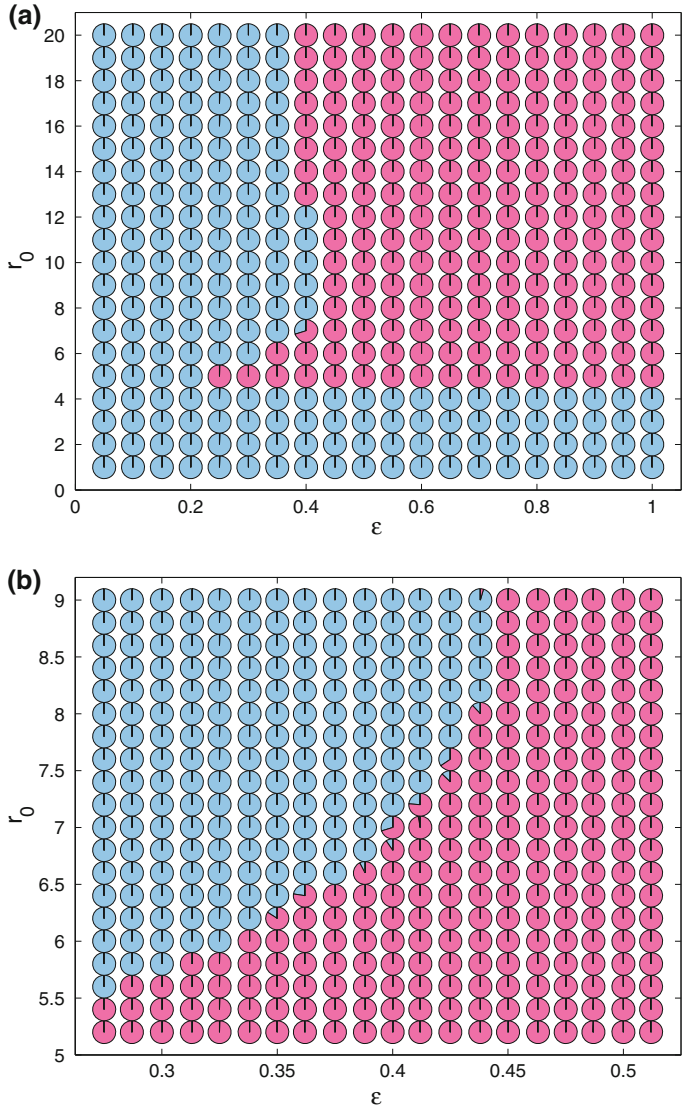

Fig. 10 In (**a**) there is a simulation diagram for $K = 0.8$ when the unforced system has oscillatory decay to the coexistence steady state. At each point tested on the (ϵ, r_0) grid, a *pie chart* shows what proportion of the 50 (or 500) simulations had a particular period. Points which showed multiple solution behaviour were run with 500 simulations for increased accuracy of the basins of attraction. The other parameters are kept constant at $a = 4\pi$, $b = 0.3$, $d = 2\pi$, $c = 1$. Each simulation was run with random initial conditions (between 0 and 1 for both prey and predator) and the period was tested after 2,000 years. The Matlab ode solver (ode15s) was run with tolerances: reltol $= 10^{-8}$ and abstol $= 10^{-6}$. The period is illustrated by the *colour with light blue* being one year cycles and *pink* being two year cycles. In the print version, one year cycles are light grey and two year cycles are darker grey. In (**b**) a close-up of the diagram to focus on the area where more than one solution appeared at the same point. This shows eleven points tested had multiple solution behaviour (colour figure online)

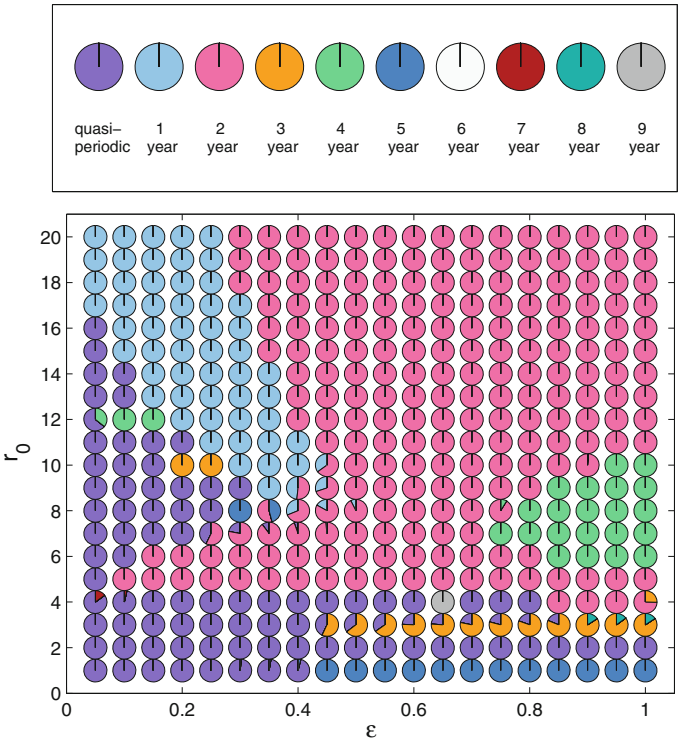

Fig. 11 A simulation diagram for $K = 1$ so that the unforced system has stable limit cycles. At each point tested on the (ϵ, r_0) grid, a *pie chart* shows what proportion of the 50 (or 500) simulations had a particular period indicated by the legend. Each simulation was run with random initial conditions (between 0 and 1 for both prey and predator) and the period was then tested after 2,000 years. The Matlab ode solver (ode15s) was run with tolerances: reltol $= 10^{-8}$ and abstol $= 10^{-6}$ (colour figure online)

At $(\epsilon, r_0) = (0.4, 7)$ in Fig. 10a, there is a pie chart indicating that multiple solution behaviour is predicted. This is close to the fold bifurcation curve in Fig. 2 and so we examine this region in more detail in Fig. 10b. We expect both one and two year solutions to be possible in the region between the fold bifurcation curve and the period-doubling curve in Fig. 2. In Fig. 10b we see that this behaviour is found through simulation at more than one grid location and the relative proportion of the two colours indicates that the two year solutions are more likely at these parameter sets. Even in the zoomed-in simulation diagram (Fig. 10b), only eleven of the pie charts show multiple solutions since the region is so small.

5.3 Simulation results for $K = 1$

We now turn to the case when there is a limit cycle present in the unforced model (Fig. 11).

In Fig. 11 one immediately notices the prominence of the two year cycles (pink). There are also large regions of one year, four year and quasi-periodic cycles. In fact,

for the most part, the behaviour is well represented by Fig. 3a, indicating that the multi-year cycles arising from the Arnol'd tongues are the minority behaviour.

All of the tongues shown in Fig. 3b are represented by some simulation results. We note that on most occasions the multi-year solution has a larger basin of attraction than the quasi-periodicity which is usually also stable at that location. In fact, often the multi-year solution attained all 50 of the simulations. The only real exception is the 7 year cycles. Furthermore, most of the multi-year cycles occur further away from the $\epsilon = 0$ axis where the tongues are thicker (again, the 7 year cycles are an exception). This is obviously due to the fact that the larger tongue means that one is more likely to capture the solution through simulation results. We reiterate here the fact that the "quasi-periodic" solutions could actually be chaotic as we do not distinguish between these cases.

There are a large number of five year cycles near $r_0 = 1$ which indicate that the five year tongue might be quite large. However, we know from Fig. 3b that the tongue is quite thin, but just happens to lie directly over the line $r_0 = 1$, which forms part of the parameter grid for our simulation. This emphasises the important point that simulation results depend significantly on the parameter grid used.

6 Different values of K

It is natural to ask how the bifurcation diagrams match up as K varies and to see if the values of K picked for each type of unforced dynamics are a good representation of the dynamics for all K values with those dynamics. We have already investigated how the period doubling curve PD2 changes for different values of K in Fig. 9. Of special interest is whether Arnol'd tongues are possible in the oscillatory decay regime. For $K = 1$, the largest of these fold bifurcation curves is the three year fold curve around $r_0 = 3$. We investigated how this curve changes as K is decreased below 1 (Fig. 12). The curve continues to exist below $K = K_2 = 0.9$: for $K = 0.85$ it lies entirely in the $\epsilon > 1$ region, and it continues to shrink as K is decreased further, disappearing entirely by $K = 0.83$, well above the switch to monotonic decay (Fig. 1). Therefore, there are Arnol'd tongues in some part of the oscillatory decay parameter regime; however, our results suggest that such folds do not occur in the monotonic decay regime.

Further, we consider how the Neimark–Sacker bifurcation curve, NS1, changes as we vary K (Fig. 13). This shows that as K decreases towards 0.9, the curve moves closer to the $\epsilon = 0$ axis. From Fig. 1 it is clear that when $K = 0.9$ there is a Hopf bifurcation for all values of r. Thus the Neimark–Sacker bifurcation is approaching the Hopf bifurcation curve as we decrease K. Figures 12 and 13 show that above $K = 0.9$ changes in K do not lead to drastic changes in the bifurcation diagrams but rather the curves vary smoothly with K. Thus we believe that our bifurcation diagram at $K = 1$ is a good representation of the bifurcation structure for all values of $K > 0.9$.

From Figs. 9, 12, 13 we see that the 2 year period-doubling curve, the 3 year fold curve and the Neimark–Sacker bifurcation curve have all disappeared for $K < 0.6$. This confirms the bifurcation work for $K = 0.35$ where only annual cycles were

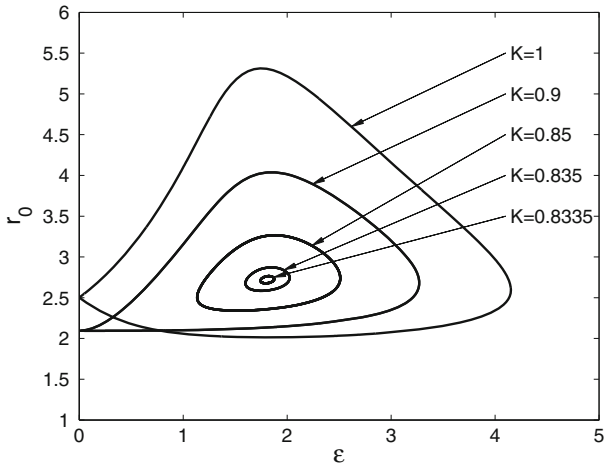

Fig. 12 The three year fold curve, as seen in Fig. 3b, is drawn in ϵ–r_0 space for different values of K. This shows the decay in the size of the tongue as K decreases past the Hopf bifurcation value ($K = 0.9$). Note that by $K = 0.85$ the fold curve only exists for $\epsilon > 1$

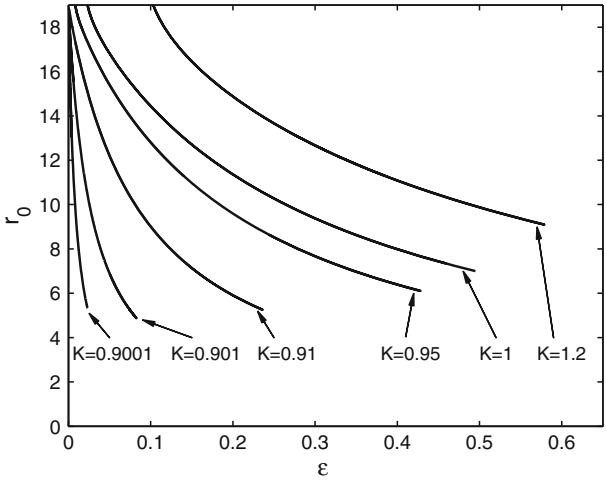

Fig. 13 The Neimark–Sacker bifurcation curve, as seen in Fig. 3a, is drawn in ϵ–r_0 space for different values of K. As K approaches $K = 0.9$ the curve smoothly approaches the $\epsilon = 0$ axis

found. It would also indicate this is a good representation of the behaviour for all values of K up to $K = 0.6$.

7 Discussion

In this paper we have investigated the dynamics of the predator–prey model (1) with forcing in the prey growth rate through the combined method of bifurcation diagrams

and simulation. This has helped to explain why cycles are occurring in different parameter regions, providing a good representation of key population behaviour and the relative frequency with which different cycles occur. Through our use of simulation that directly corresponds to the bifurcation diagrams we have provided a further tool for understanding these diagrams.

Our choice of prey growth rate as the forced parameter has enabled us to separate the cases of oscillatory decay and limit cycles, in contrast with forcing parameters involved in the condition for a Hopf bifurcation in the unforced system (Rinaldi et al. 1993). This has led to a clear understanding of the dependence of cycles on the underlying oscillatory nature of the unforced model, highlighting the fact that the level of oscillation in the unforced system has a large effect on the range of possible behaviour. Specifically we have shown that when the unforced dynamics of the model exhibits monotonic decay or oscillatory decay, with low amplitude oscillations, to the coexistence steady state, the forced system will exhibit annual cycles which follow the forcing oscillation only. When the unforced system exhibits limit cycles or a sufficient level of oscillatory decay, multi-year cycles are induced due to seasonal forcing. However, the limit cycles case showed a much richer range of behaviour. This includes coexisting multi-year cycles, quasi-periodicity and chaos, particularly when the forcing strength is high. This is in keeping with the work of Rinaldi and co-workers (Rinaldi et al. 1993; Rinaldi and Muratori 1993; Gragnani and Rinaldi 1995). This does not rule out Arnol'd tongues occurring for the cases where multi-year cycles are induced in the oscillatory decay system: these do occur (Fig. 12), and they are often seen in epidemiological models, which do not have limit cycles in the absence of forcing (Kuznetsov and Piccardi 1994; Greenman et al. 2004; Childs and Boots 2010). However, our results highlight the particular importance of studying systems under the influence of seasonal forcing which are intrinsically cyclic, as they may be able to exhibit a wider range of population behaviour.

For both the limit cycle and oscillatory decay case, the range of behaviour that we have found includes (for some parameters) coexisting multi-year cycles of different periods. However, the limit cycle case showed this more frequently than the oscillatory decay case, as well as having parameter regions where coexisting multi-year cycles of the same period occurred. In general, the limit cycle case exhibited more variety and a larger area of parameter space resulted in non-annual behaviour. We also found (in the limit cycle case) the unintuitive phenomenon of increasing forcing leading to more regular behaviour (Fig. 3). This occurred when a higher forcing amplitude led to stability of the yearly cycle instead of the quasi-periodic cycle.

The onset of cycles, in terms of the forcing parameters r_0 and ϵ, was dependent on the unforced dynamics of the system. In the oscillatory decay case, a significant level of forcing was required in order to produce subharmonics. In the limit cycle case, non-annual cycles occurred for low levels of forcing, such as the parameter region giving quasi-periodic solutions and the Arnol'd tongues which touch the $\epsilon = 0$ axis (Fig. 3b). However, in reality most of the tongues are so thin near the axis that the solutions are hard to distinguish from quasi-periodic behaviour unless the amplitude of forcing is increased. Also of note is that in the oscillatory decay regime, multi-year cycles occur for higher values of r_0 compared to the limit cycle case. The robustness of this result to changes in other model parameters is a natural area for future work.

There are many examples where multi-year cycles occur in natural populations, especially in insect, plankton and small mammal systems (Kendall et al. 1999; Turchin 2003). *Daphnia pulex* and its algal prey *Chlamydonomas reinhardii* is one system where the behaviour is cyclic (Nisbet et al. 1991; McCauley et al. 1999; McCauley and Murdoch 1987) and where seasonal forcing has been implicated as an important driver of the dynamical behaviour (Scheffer et al. 1997). Moreover, this predator–prey interaction has been studied and parameterised in detail (Nisbet et al. 1991). Therefore it makes a natural test system for further study with the growth rate of the algae forced by changing light conditions in a similar manner to the fish-plankton model of Doveri et al. (1993). Many small mammal systems also show multi-year cycles (Turchin 2003). A number of different mechanisms have been proposed as the cause of this cyclic behaviour, but for the well-studied case of Fennoscandian voles, predator-exclusion experiments have shown that the multi-year cycles in the northern areas depend fundamentally on predation (Korpimaki and Norrdahl 1998; Korpimaki et al. 2002; Hanski et al. 2001). At these northern latitudes, which have a higher degree of seasonality in the environment, vole abundance fluctuates with period 3–5 years (Turchin 2003; Hanski et al. 2001). As one moves further south, there is a switch to annual fluctuations (Hanski et al. 2001) attributed to a change in predation from specialist predators (weasels) to generalist predators (e.g. birds, foxes) (Hanski et al. 1993; Turchin and Hanski 1997). The methods described in this manuscript could be extended to consider the relative effects of specialist and generalist predation in conjunction with the impact of seasonality to determine the influence of changes in the degree of seasonality on population behaviour.

Many extensions of this work could be undertaken to enhance biological realism and to further our understanding of the effects of seasonal forcing, including forcing more than one parameter, in particular with different phases and forcing strengths (Rinaldi and Muratori 1993; Greenman and Pasour 2011). Moreover, adaptations could be made to the forcing term in order to add more realism into the model. Instead of a sinusoidal term, step functions have been used to represent a defined breeding season although this tends to yield similar results (Ireland et al. 2004). Other possibilities could be to alter the sinusoidal term to consider different breeding season lengths or to consider chaotic forcing (Greenman and Norman 2007; Colombo et al. 2008). Furthermore, this approach could be applied to a wide range of biological systems including tritrophic food chains (Kuznetsov et al. 2001), disease systems (Kuznetsov and Piccardi 1994; Earn et al. 2000; Greenman et al. 2004) and invading populations (Webb and Sherratt 2004; Greenman and Norman 2007).

These, and other population systems, highlight the importance of studying seasonal forcing in systems with cyclic dynamics. Cyclic predator–prey systems in the real world require careful analysis to determine the origin of those cycles, and this analysis must recognise that these cycles could be highly dependent on the seasonality inherent in their environment.

Acknowledgments R. A. Taylor was funded by a Doctoral Training Account studentship from EPSRC. J. A. Sherratt was funded in part by a Research Fellowship from Leverhulme Trust. The authors wish to thank Jon Greenman for helpful discussions.

References

Altizer S, Dobson A, Hosseini P, Hudson P, Pascual M, Rohani P (2006) Seasonality and the dynamics of infectious diseases. Ecol Lett 9:467–484

Bolzoni L, Dobson A, Gatto M, De Leo GA (2008) Allometric scaling and seasonality in the epidemics of wildlife diseases. Am Nat 172:818–828

Childs DZ, Boots M (2010) The interaction of seasonal forcing and immunity and the resonance dynamics of malaria. J R Soc Interface 7:309–319

Choisy M, Guegan JF, Rohani P (2006) Dynamics of infectious diseases and pulse vaccination: teasing apart the embedded resonance effects. Phys D 223:26–35

Colombo A, Dercole F, Rinaldi S (2008) Remarks on metacommunity synchronization with application to prey-predator systems. Am Nat 171:430–442

Dietz K (1976) The incidence of infectious disease under the influence of seasonal fluctuations. In: Lecture notes in biomathematics: mathematical models in medicine, vol 11. Springer, Berlin, pp 1–15

Doedel EJ (1981) AUTO: a program for the automatic bifurcation analysis of autonomous systems. Congr Numer 30:265–384

Doedel EJ, Oldeman BE (2009) AUTO-07P: continuation and bifurcation software for ordinary differential equations. Manual. http://indy.cs.concordia.ca/auto

Doedel EJ, Keller HB, Kernevez JP (1991) Numerical analysis and control of bifurcation problems: (I) bifurcation in finite dimensions. Int J Bifurcat Chaos 1:493–520

Doedel EJ, Govaerts W, Kuznetsov YA, Dhooge A (2006) Numerical continuation of branch points of equilibria and periodic orbits. In: Modelling and computations in dynamical systems. World Scientific, Singapore, pp 145–164

Doveri F, Scheffer M, Rinaldi S, Muratori S, Kuznetsov Y (1993d) Seasonality and chaos in a Plankton-Fish model. Theor Popul Biol 43:159–183

Dushoff J, Plotkin J, Levin S, Earn D (2004) Dynamical resonance can account for seasonality of influenza epidemics. Proc Natl Acad Sci USA 101:16915–16916

Earn DJD, Rohani P, Bolker BM, Grenfell BT (2000) A simple model for complex dynamical transitions in epidemics. Science 287:667–670

Finkenstadt BF, Grenfell BT (2000) Time series modelling of childhood diseases: a dynamical systems approach. J R Stat Soc Ser C Appl Stat 49:187–205

Giesl P (2007) Construction of global Lyapunov functions using radial basis functions. Springer, Berlin

Gragnani A, Rinaldi S (1995) A universal bifurcation diagram for seasonally perturbed predator-prey models. Bull Math Biol 57:701–712

Greenman JV, Benton TG (2004) Large amplification in stage-structured models: Arnol'd tongues revisited. J Math Biol 48:647–671

Greenman J, Norman R (2007) Environmental forcing, invasion and control of ecological and epidemiological systems. J Theor Biol 247:492–506

Greenman JV, Pasour VB (2011) Phase control of resonant systems: interference, chaos and high periodicity. J Theor Biol 278:74–86

Greenman JV, Kamo M, Boots M (2004) External forcing of ecological and epidemiological systems: a resonance approach. Phys D 190:135–151

Guckenheimer J, Holmes P (1983) Nonlinear oscillations, dynamical systems and bifurcations of vector fields. Springer, Berlin

Hanski I, Turchin P, Korpimaki E, Henttonen H (1993) Population oscillations of boreal rodents: regulation by mustelid predators leads to chaos. Nature 364:232–235

Hanski I, Henttonen H, Korpimaki E, Oksanen L, Turchin P (2001) Small-rodent dynamics and predation. Ecology 86:1505–1520

He D, Earn DJD (2007) Epidemiological effects of seasonal oscillations in birth rates. Theor Popul Biol 72:274–291

Holt J, Colvin J (1997) A differential equation model of the interaction between the migration of the Senegalese grasshopper, *Oedaleus senegalensis*, its predators, and a seasonal habitat. Ecol Model 101: 185–193

Ireland JM, Norman RA, Greenman JV (2004) The effect of seasonal host birth rates on population dynamics: the importance of resonance. J Theor Biol 231:229–238

Keeling MJ, Rohani P (2008) Modelling infectious diseases in humans and animals. Princeton University Press, Princeton

Kendall BE, Briggs CJ, Murdoch WW, Turchin P, Ellner SP, McCauley E, Nisbet R, Wood SN (1999) Why do populations cycle? A synthesis of statistical and mechanistic modelling approaches. Ecology 80:1789–1805

King AA, Schaffer WM (1999) The rainbow bridge: Hamitonian limits and resonance in predator-prey dynamics. J Math Biol 39:439–469

King AA, Schaffer WM (2001) The geometry of a population cycle: a mechanistic model of snowshoe hare demography. Ecology 82:814–830

Korpimaki E, Norrdahl K (1998) Experimental reduction of predators reverses the crash phase of small-rodent cycles. Ecology 79:2448–2455

Korpimaki E, Norrdahl K, Klemola T, Petterson T, Stenseth NC (2002) Dynamic effects of predators on cyclic voles: field experimentation and model extrapolation. Proc R Soc B 269:991–997

Kuznetsov YA (1995) Elements of applied bifurcation theory. Springer, New York

Kuznetsov YA, Piccardi C (1994) Bifurcation analysis of periodic SEIR and SIR epidemic models. J Math Biol 32:109–121

Kuznetsov YA, Muratori S, Rinaldi S (1992) Bifurcations and chaos in a periodic predator-prey model. Int J Bifurcat Chaos 2:117–128

Kuznetsov YA, De Feo O, Rinaldi S (2001) Belyakov homoclinic bifurcations in a tritrophic food chain model. SIAM J Appl Math 62:462–487

Mabille G, Descamps S, Berteaux D (2010) Predation as a probable mechanism relating winter weather to population dynamics in a North American Porcupine population. Popul Ecol 52:537–546

Mancusi E, Russo L, Continillo G, Crescitelli S (2004) Computation of frequency locking regions for a discontinuous periodically forced reactor. Comput Chem Eng 28:187–194

McCauley E, Murdoch WW (1987) Cyclic and stable populations: plankton as paradigm. Am Nat 129: 97–121

McCauley E, Nisbet RM, Murdoch WW, de Roos AM, Gurney W (1999) Large-amplitude cycles of Daphnia and its algal prey in enriched environments. Nature 402:653–656

Nisbet R, McCauley E, De Roos AM, Murdoch WW, Gurney W (1991) Population dynamics and element recycling in an aquatic plant-herbivore system. Theor Popul Biol 40:125–147

Rinaldi S, Muratori S (1993) Conditioned chaos in seasonally perturbed predator-prey models. Ecol Model 69:79–97

Rinaldi S, Muratori S, Kuznetsov YA (1993) Multiple attractors, catastrophes and chaos in seasonally perturbed predator-prey communities. Bull Math Biol 55:15–35

Rosenzweig M, MacArthur R (1963) Graphical representation and stability conditions of predator-prey interactions. Am Nat 97:209–223

Schaffer WM, Pederson BS, Moore BK, Sharpaas O, King AA, Bronnikova TV (2001) Sub-harmonic resonance and multi-annual oscillations in Northern Mammals: a non-linear dynamical systems perspective. Chaos Soliton Fract 12:251–264

Scheffer M, Rinaldi S, Kuznetsov YA, van Nes EH (1997) Seasonal dynamics of Daphnia and algae explained as a periodically forced predator-prey system. OIKOS 80:519–532

Seydel R (1994) Practical bifurcation and stability analysis, 2nd edn. Springer, New York

Smith MJ, White A, Sherratt JA, Telfer S, Begon M, Lambin X (2008) Disease effects on reproduction can cause population cycles in seasonal environments. J Anim Ecol 77:378–389

Stenseth NC, Bjornstad ON, Saitoh T (1998) Seasonal forcing on the dynamics of *Clethrionomys rufocanus*: modeling geographic gradients in population dynamics. Res Popul Ecol 40:85–95

Turchin P (2003) Complex population dynamics. Princeton University Press, Princeton

Turchin P, Hanski I (1997) An empirically based model for latitudinal gradient in vole population dynamics. Am Nat 149:842–874

Webb SD, Sherratt JA (2004) Oscillatory reaction-diffusion equations with temporally varying parameters. Math Comput Model 39:45–60